



HAL
open science

Gaseous ozone decomposition over high silica zeolitic frameworks

Nicolas Brodu, Marie-Hélène Manero, Caroline Andriantsiferana,
Jean-Stéphane Pic, Héctor Valdés

► **To cite this version:**

Nicolas Brodu, Marie-Hélène Manero, Caroline Andriantsiferana, Jean-Stéphane Pic, Héctor Valdés. Gaseous ozone decomposition over high silica zeolitic frameworks. *Canadian Journal of Chemical Engineering*, 2018, 96 (9), pp.1911-1918. 10.1002/cjce.23141 . hal-01963225

HAL Id: hal-01963225

<https://hal.science/hal-01963225v1>

Submitted on 21 Dec 2018

HAL is a multi-disciplinary open access archive for the deposit and dissemination of scientific research documents, whether they are published or not. The documents may come from teaching and research institutions in France or abroad, or from public or private research centers.

L'archive ouverte pluridisciplinaire **HAL**, est destinée au dépôt et à la diffusion de documents scientifiques de niveau recherche, publiés ou non, émanant des établissements d'enseignement et de recherche français ou étrangers, des laboratoires publics ou privés.





Open Archive Toulouse Archive Ouverte

OATAO is an open access repository that collects the work of Toulouse researchers and makes it freely available over the web where possible

This is an author's version published in: <http://oatao.univ-toulouse.fr/21081>


Official URL: <https://doi.org/10.1002/cjce.23141>

To cite this version:

Brodu, Nicolas and Manero, Marie-Hélène  and Andriantsiferana, Caroline  and Pic, Jean-Stéphane and Valdés, Héctor *Gaseous ozone decomposition over high silica zeolitic frameworks*. (2018) *The Canadian Journal of Chemical Engineering*, 96 (9). 1911-1918. ISSN 0008-4034

Any correspondence concerning this service should be sent to the repository administrator: tech-oatao@listes-diff.inp-toulouse.fr

GASEOUS OZONE DECOMPOSITION OVER HIGH SILICA ZEOLITIC FRAMEWORKS

Nicolas Brodu ^{1*} Marie-Hélène Manero,² Caroline Andriantsiferana,² Jean-Stéphane Pic³ and Héctor Valdés⁴

1. Normandie Univ, UNIROUEN, INSA Rouen, LSPC, 76000 Rouen, France

2. Laboratoire de Génie Chimique, Université de Toulouse, CNRS, INPT, UPS, Toulouse, France

3. LISBP, Université de Toulouse, CNRS, INRA, INSA, Toulouse, France

4. Laboratorio de Tecnologías Limpias (F. Ingeniería), Universidad Católica de la Santísima Concepción, Alonso de Ribera 2850, Concepción, Chile

For several decades, it has been known that ozone emissions are harmful to humans, plants, and animals. Heterogeneous catalytic decomposition is an efficient process for removing ozone from air. This study examines the effect of the zeolite's framework and pore width on efficiency for decomposing gaseous ozone. Four highly hydrophobic zeolites are used: a large cavity zeolite (Faujasite/H FAU), a medium pore zeolite with parallel channel (Mordenite/H MOR), and two medium pore zeolites with interconnected channels (H ZSM 5/H MFI and Na ZSM 5/Na MFI). Experiments were conducted in fixed bed flow reactors loaded with zeolite at ambient conditions (20 °C and 101 kPa). Zeolite surfaces were analyzed during the experiments in order to understand the influence of physical and chemical surface properties on the ozone decomposition mechanism. A higher amount of ozone is eliminated using H MOR, compared with the zeolite samples H FAU, H MFI, and Na MFI. Pore width and micropore framework size distribution (channel and cages) appear to be key factors. A narrow channel or cage, slightly larger than the ozone molecule size, seems to promote ozone interactions with Lewis acid sites. Fourier transform infrared spectroscopy shows that Lewis acid sites (LAS), located on the walls of zeolite pores, decompose ozone. This leads to the formation of atomic oxygen species that could react with another ozone molecule to form dioxygen. Hence, LAS are regenerated, ready to decompose another ozone molecule once more.

Keywords: ozone, zeolite framework, Lewis acidity, pore width

INTRODUCTION

Numerous toxic molecules deteriorate ambient air quality. One of them is ozone, which is known to have harmful effects on human health, living organisms, and the environment.^[1,2] Ozone is present in the contaminated air of urban areas, acting as a secondary pollutant, as well as in working environments, mainly due to the use of photocopiers and laser printers. Ozone is also a strong oxidant widely used in wastewater treatment, air purification, and sterilization of waste.^[3] During such processes, the concentration of residual ozone in exhaust streams is generally much higher than the value recommended by the World Health Organization.^[4]

In order to meet air quality standards, local abatement systems have to be implemented to eliminate residual ozone. To remove this pollutant, decomposition using solid microporous materials has been identified as effective.^[5-7] Several authors have shown interesting removal efficiencies when activated carbons are used to decompose gaseous ozone. However, a degradation of activated carbon structure has also been proven.^[5,8,9] Hence, materials that are more resistant have to be found. Metal oxides such as manganese or silver oxides have been reported to be very efficient in ozone decomposition.^[4,9] Nevertheless, the performances of such materials are strongly limited due to their low active surface. A combination of both high specific surface and high catalytic properties are necessary to destroy ozone. Aluminosilicates could be good alternative materials, as they have high specific surfaces and are resistant toward ozone attacks.

Recently, some studies reported the interest of using microporous zeolites as supports for metal oxide catalysts.^[10-17] However, there is very little information on the decomposition of gaseous

ozone by pure zeolites without any metal oxide deposit. The efficiency of ozone decomposition largely depends on the physico-chemical properties of the materials. It has been found that high silica zeolites have the ability to adsorb gaseous ozone.^[18] Several works show the key role played by the surface acid sites.^[5,7,19-21] The contribution of Brønsted and Lewis acid sites has been investigated for the decomposition of ozone. Valdés et al.^[21] claimed that adsorption of ozone could occur at strong and weak Lewis acid sites. Other studies^[7,19,20] have suggested that ozone decomposition only operates on strong Lewis acid sites, with a similar mechanism reported for aluminium oxide material.^[22] In specific cases of zeolites having been subjected to a dealumination step, the decomposition of zeolite can also be attributed to silanol groups.^[18,23]

There are 206 registered unique zeolite frameworks with different geometric parameters and compositions.^[24] Hence, the most influential physical and chemical properties of zeolites towards ozone decomposition should be identified. The effects of microporous and mesoporous materials such as H-Beta and MCM-41 on ozone elimination have been reported.^[11] However, there are still some doubts related to the influence of zeolite framework on ozone removal. This study aims to understand the influence of

physical and chemical surface properties of high silica zeolites on ozone decomposition mechanism. Four synthetic hydrophobic zeolites with three different kinds of framework and chemical composition are selected. The following questions are addressed: what is the role of pore size and framework structure? Do acidic sites play the same role for all kind of zeolites?

MATERIALS AND METHODS

Materials

Four hydrophobic zeolites with different framework structures are studied: a Mordenite type (H-MOR from *Tosoh*), a Faujasite type (H-FAU from *Tosoh*), and two ZSM-5 types (MFI from *zeochem* and *Tosoh*). ZSM-5 zeolites present different content of compensating cations (Na-MFI and H-MFI) and $\text{SiO}_2/\text{Al}_2\text{O}_3$ ratios. Zeolite samples were received as pellets. For some

experiments, zeolite pellets were ground and sieved at the same particle size (0.300–0.425 mm). In others, they were used in their original form and size. A thermal out-gassing procedure was applied to all zeolites. They were thermally out-gassed at 500 °C for 6 h, prior to ozone decomposition experiments.

Figure 1 illustrates schematic representations of zeolite frameworks used in this study. Zeolite frameworks are composed of channels and cages. The micropore structure of mordenite type zeolite consists of 12-membered straight channels and apertures of 0.65×0.7 nm with the presence of side pockets (0.26×0.57 nm).^[25] Faujasite type zeolite consists of cubicoctahedrons called sodalite cages.^[25] The assembly of sodalite cages linked together gives 1.3 nm diameter supercages interconnected with pore apertures of 0.74 nm diameter. ZSM-5 exhibits a three-dimensional pore network, which has a 10-membered [oxygen] ring system. Its framework contains two perpendicularly intersecting channel systems 0.53×0.56 nm and 0.51×0.55 nm in size, respectively. Intersections are

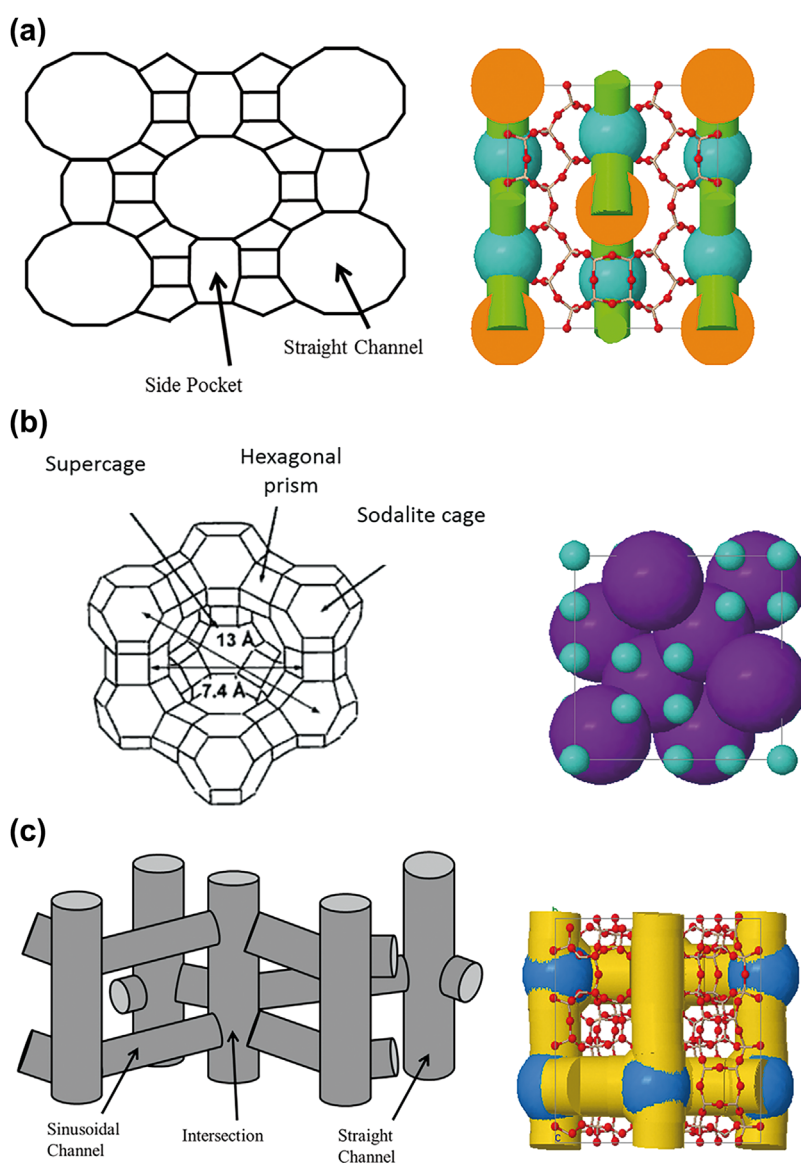


Figure 1. Schematic representations of zeolite structures (on the left)^[27,28] and topologies (on the right):^[29] (a) H MOR, (b) H FAU, and (c) ZSM 5. In the topologic schemes, spherical forms represent cage structure, cylinder forms stand for channel structure, and red atoms are oxygen molecules.

characterized by 0.8 nm diameter cages.^[26] Faujasite structure is more open than that of mordenite and ZSM-5.

Physical-Chemical Surface Characterization of Zeolites

Specific surface areas and pore volumes were obtained by Nitrogen adsorption-desorption at 196 °C using a *Micromeritics ASAP 2010* instrument. Prior to nitrogen adsorption, zeolite samples were out-gassed at 90 °C for 1 h and then at 350 °C for 4 h. Specific surface areas (S_{BET}) were calculated from nitrogen adsorption isotherms, using the Brunauer–Emmett–Teller (BET) equation.^[30] Micropore volume (V_{micro}) were obtained by applying the Horvath-Kawazoe (HK) method.^[31]

Lewis and Bronsted acid site concentrations were determined by Infra-Red (IR) spectroscopy using pyridine as a probe molecule (99.5 % purity supplied by *Fluka*; kinetic diameter of 0.52 nm). Measurements were performed using a *NICOLET MAGNA IR 550* spectrometer equipped with a vacuum cell. Zeolite samples were pressed into thin wafers (10 mg cm⁻²) and were activated in situ in the IR cell, passing air flow (1 cm³ s⁻¹) at 450 °C for 12 h and then applying vacuum (1.33 × 10⁻⁴ Pa) at 400 °C for 1 h. After the adsorption of pyridine at 150 °C, a thermal desorption procedure was conducted (steps from 150 °C to 450 °C).^[20] The concentration of Lewis acid sites and Bronsted acid sites were calculated by evaluating the amount of remaining pyridine after the applied thermal desorption procedure by the integration of the IR bands at 1444–1454 cm⁻¹ and 1545 cm⁻¹, using 1.28 cm · mol⁻¹ and 1.13 cm · mol⁻¹ as molar absorption coefficients, respectively.^[32] Detailed information on the procedures and calculations can be found elsewhere.^[20,33]

Experimental Setup

Ozone removal experiments were conducted using two reactors of different sizes: (i) a small fixed-bed flow reactor (4 mm ID), loaded with zeolite samples ($m = 0.1$ g; particle size between 0.3–0.425 mm); (ii) a big fixed-bed flow reactor (45 mm ID, 150 mm long), filled with pellet zeolites ($m = 44$ g, particle size of 1.8 mm). The first system (i) was previously described by Brodu et al.^[20] Dry ozonated air was sent through the zeolite bed. In the second system, ozone was generated from dry air using a Labo 5LO ozone generator (*Trailgaz*). Prior to any ozone contact, the mass of the reactor loaded with the zeolite sample was measured, using a technical balance (Mettler ME4001TE). After different exposition times towards gaseous ozone, the reactor charged with the zeolite sample was disconnected from the experimental system and the increase in the zeolite mass was determined. In parallel, zeolite samples were analyzed by FTIR spectroscopy.

In both systems, the exhaust gas stream was sent to an ozone trap before discharging to ambient air. All experiments were conducted at 20 °C (± 1 °C) and 101 kPa. Ozone inlet concentration ranged from 5 to 26 g · m⁻³. The evolution of the outlet concentration of ozone was recorded continuously using a *BMT 964* ozone analyzer. Total amount of removed ozone, q_{O_3} (g_{O3} · g_{zeolite}⁻¹), was calculated from a mass balance between the inlet and the outlet reactor stream using Equation (1), as follows:

$$q_{O_3} = \frac{F}{m} \int_0^{t_0} \left(1 - \frac{O_{3t}}{O_{3in}} \right) dt \quad (1)$$

where m is the mass of zeolite in the fixed bed (g); O_{3in} is the inlet concentration of ozone (g · m⁻³); F is the volumetric flow rate

(m³ · min⁻¹); t_0 is the time needed to reach the inlet ozone concentration at the outlet stream (min); O_{3t} and is the ozone concentration as a function of time (g · m⁻³).

Study of Surface Interaction between Zeolite Samples and Ozone

The evolution of ozone intermediates on zeolite surfaces during ozone decomposition experiments was analyzed by Fourier transform infrared (FTIR) spectroscopy using a *BRUKER TENSOR 27* spectrometer. Zeolite samples were taken after ozone contact in the big fixed-bed flow reactor (internal diameter of 45 mm). Prior to analysis, zeolite samples were ground and compacted to form a thin wafer. Spectra were recorded with a resolution of 2 cm⁻¹ ranging from 1300 to 1750 cm⁻¹.^[34]

RESULTS AND DISCUSSION

Characterization of As-Received Zeolites

Table 1 shows topological information corresponding to the four studied zeolites. Free sphere diameter (D_i) corresponds to the largest spherical molecule that can enter into a zeolite channel.^[24] Maximum included sphere diameter (D_{max}) represents the largest spherical molecule that can be placed inside a zeolite cage.^[24,35] As expected, for each zeolite, the value of D_i is lower than the value of D_{max} . A high difference for H-FAU zeolite ($D_i = 0.74$ nm and $D_{max} = 1.3$ nm) can be observed, showing the importance of the size of the cages of this zeolite, as is shown in Figure 1. H-MOR zeolite presents a rather different structure, with two types of cages. The smaller one, named side pockets (P) (0.26 × 0.57 nm), corresponds to 41 % of the microporous volume.^[25] As the size of ozone molecules (0.58 nm)^[34] is larger than the size of these cages, only straight channels of this material are accessible. The micropore structure of ZSM-5 zeolites (Na-MFI, H-MFI) includes straight, sinusoidal channels (C), as well as intersections (I). For this kind of zeolite, the channels represent 59 % of the available micropore volume.^[34] Although the D_i value is slightly smaller than the ozone molecule size, ozone molecules could still enter into the pores because of its structure vibration.^[36]

Table 1 also lists other physical characteristics of zeolite samples such as S_{BET} and micropore volumes, V_{micro} , corresponding to channels and/or intersections. It can be noted that H-MOR and H-FAU zeolites have similar BET surfaces and micropore volumes. Nevertheless, only the channel volume of H-MOR (0.11 cm³ · g⁻¹) is accessible to ozone molecules. Thus, available micropore volume of H-MOR zeolite is quite close to the micropore volumes of both ZSM-5 zeolites. Lewis and Brønsted acid site concentrations are presented in Table 1. In the case of H-MOR, only acidic sites at the surface of straight channels of H-MOR zeolite can be detected. Indeed, pyridine molecules are too large (0.52 nm) to enter the small pockets of H-MOR zeolite (0.26 × 0.57 nm).^[37] Lewis acid sites have been claimed to be the main surface sites responsible for ozone decomposition.^[7,34] They have been detected in all zeolites and their concentrations range from 28 to 91 μmol · g⁻¹. H-MOR zeolite presents the highest amount of Lewis acid sites, whereas H-MFI zeolite has the smallest content. Lewis acid site concentration of Na-MFI is almost two times higher than the value of the H-MFI sample. Concerning Brønsted acid sites, both kinds of ZSM-5 samples have a lower concentration than H-FAU and H-MOR zeolites. However, it has already been reported that these sites are not active for ozone decomposition.^[7,33]

Table 1. Physical and chemical surface properties of zeolite samples

Sample	CR	CC	MR	nD ^a ()	D _{max} (nm)	D _i (nm)	Pore diameter (nm)	SiO ₂ /Al ₂ O ₃ ratio	V _{micro} ^b (cm ³ .g ⁻¹)	Available V _{micro} ^c (cm ³ .g ⁻¹)	S _{BET} (m ² . g ⁻¹)	Lewis acid sites ^d (μmol.g ⁻¹)	Bronsted acid sites ^d (μmol.g ⁻¹)
H-MOR	MOR	H ⁺	12	1	0.67	0.65	Pocket (P): 0.26 × 0.57 Channel (C): 0.65 × 0.7	230	P: 0.10 C: 0.11	0.11	508	91	110
H-FAU	FAU	H ⁺	12	3	1.3	0.74	1.3	14	0.20	0.20	528	67	67
Na-MFI	MFI	Na ⁺	10	3	0.64	0.47	Intersection (I): 0.6 × 0.8 Channels (C): 0.51 × 0.55 & 0.53 × 0.56	360	I: 0.049 C: 0.071	0.12	309	53	5
H-MFI	MFI	H ⁺	10	3	0.64	0.47		2100	I: 0.035 C: 0.065	0.11	308	28	4

CR: Code structure; CC: Compensating cations; MR: number of member ring; nD: Pore dimension; D_i: Maximum free sphere diameter; D_{max}: Maximum include sphere diameter

^aGeometry dimension of the framework created by pores and channels of the zeolite

^bDetermined from nitrogen adsorption isotherms at 196 °C

^cMicropore volume accessible to ozone and pyridine molecules

^dObtained from IR spectra after adsorption/desorption of pyridine

Influence of Zeolite Chemical Features on Ozone Decomposition

Results of gaseous ozone elimination over zeolites are obtained from experiments conducted in the small reactor (4 mm ID) loaded with ground zeolite (particle size of 0.3–0.425 mm). Figure 2 shows the evolution of the outlet ozone dimensionless concentration as a function of time during the contact with four zeolite samples, using an inlet ozone concentration of 15 g · m⁻³. In the case of both ZSM-5 zeolites (Na-MFI and H-MFI), the breakthrough curves increase rapidly, remaining close for 35 min; then the increase proceeds at a slower rate. These rapid changes in the breakthrough curves could be explained by the pore sizes of ZSM-5 zeolite. The value of D_i (0.47 nm) is lower than the size of ozone molecule (0.58 nm). Ozone diffusion inside pore channels seems to be sterically limited. The total amounts of ozone eliminated, calculated using Equation (1), are 0.52 g_{O₃} · g_{zeolite}⁻¹ and 0.22 g_{O₃} · g_{zeolite}⁻¹ for Na-MFI and H-MFI, respectively. This difference could be due to the higher concentration of Lewis acid sites of the Na-MFI sample compared to the H-MFI sample. Indeed, the ratio between the amount of ozone eliminated using Na-MFI zeolite and the amount of ozone removed over the H-MFI sample (0.52/0.22 = 2.3) is close to the ratio of the concentration of Lewis acid sites between the Na-MFI zeolite and H-MFI zeolite (53/28 = 1.9).

In the case of H-FAU and H-MOR samples, ozone in the outlet stream is first observed at 80 min and at 100 min, respectively. H-MOR and H-FAU zeolites show a complete elimination of ozone. In these cases, the values of D_i are larger than the size of ozone molecule. Therefore, ozone could easily diffuse into the pores of these zeolites and could be in contact with active surface sites that lead to ozone decomposition. In comparison to both ZSM-5 samples (Na-MFI and H-MFI), better performances are obtained with these zeolites: 2.05 g_{O₃} · g_{zeolite}⁻¹ for H-MOR and 0.75 g_{O₃} · g_{zeolite}⁻¹ for H-FAU, in accordance with their Lewis acid contents (91 μmol.g⁻¹ and 73 μmol.g⁻¹, respectively).

Thus, two different behaviours are observed. At the beginning of ozone contact, no ozone is registered at the reactor outlet stream. Under this condition, ozone could be adsorbed and decomposed at active Lewis acid sites of the zeolite surface. As the exposition time increases, when the outlet concentration of ozone gradually reaches the inlet concentration of ozone, zeolites lose their activity to eliminate ozone. Zeolite active sites could be poisoned. Active surface

sites of zeolite surface could be exposed to other chemical compounds beside ozone that could block the interaction with ozone molecules.

Ozone Interaction with Zeolite Surface Sites

Results of ozone interactions with the zeolite surface are studied by FTIR spectroscopy using zeolite samples taken from the big fixed-bed reactor (45 mm ID) loaded with pellet zeolites (particle size of 1.8 mm). The evolution of FTIR spectra of three different zeolite framework structures after ozone contact are shown in Figures 3A (H-MOR), 3B (H-FAU), and 3C (Na-MFI). Additionally, the variation of zeolite bed mass and the temperature of the reactor external wall as a function of exposition time towards ozone are registered during the same assays, and results of mass change are plotted in Figure 4.

Regardless of the kind of zeolite used, a band at 1384 cm⁻¹ is detected for all samples and has been identified as atomic oxygen adsorbed on Lewis acid sites.^[34] Two phases of ozone elimination are clearly distinguished for H-MOR and Na-MFI. The first one is from 0 to 170 min for H-MOR and from 0 to 220 min for Na-MFI. The second phase starts at 170 min (H-MOR) and 220 min (Na-MFI) and lasts until the end. In the case of H-FAU zeolite, the first phase is not clearly observed due to insufficient samples taken during this phase. Thus, it is not

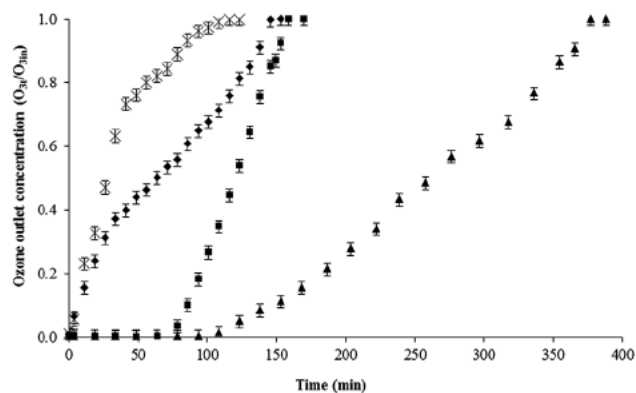


Figure 2. Influence of zeolite properties on ozone removal: (▲) H MOR, (■) H FAU, (◆) Na MFI, (×) H MFI. Operating conditions: 0.1 g of ground zeolite with particle size in the range of 0.3–0.425 mm; O_{3in}: 15 g · m⁻³; F: 0.003 m³ · h⁻¹; 101 kPa; 20 °C; O_{3t}/O_{3in} represents the variation of dimensionless concentration of ozone as a function of time.

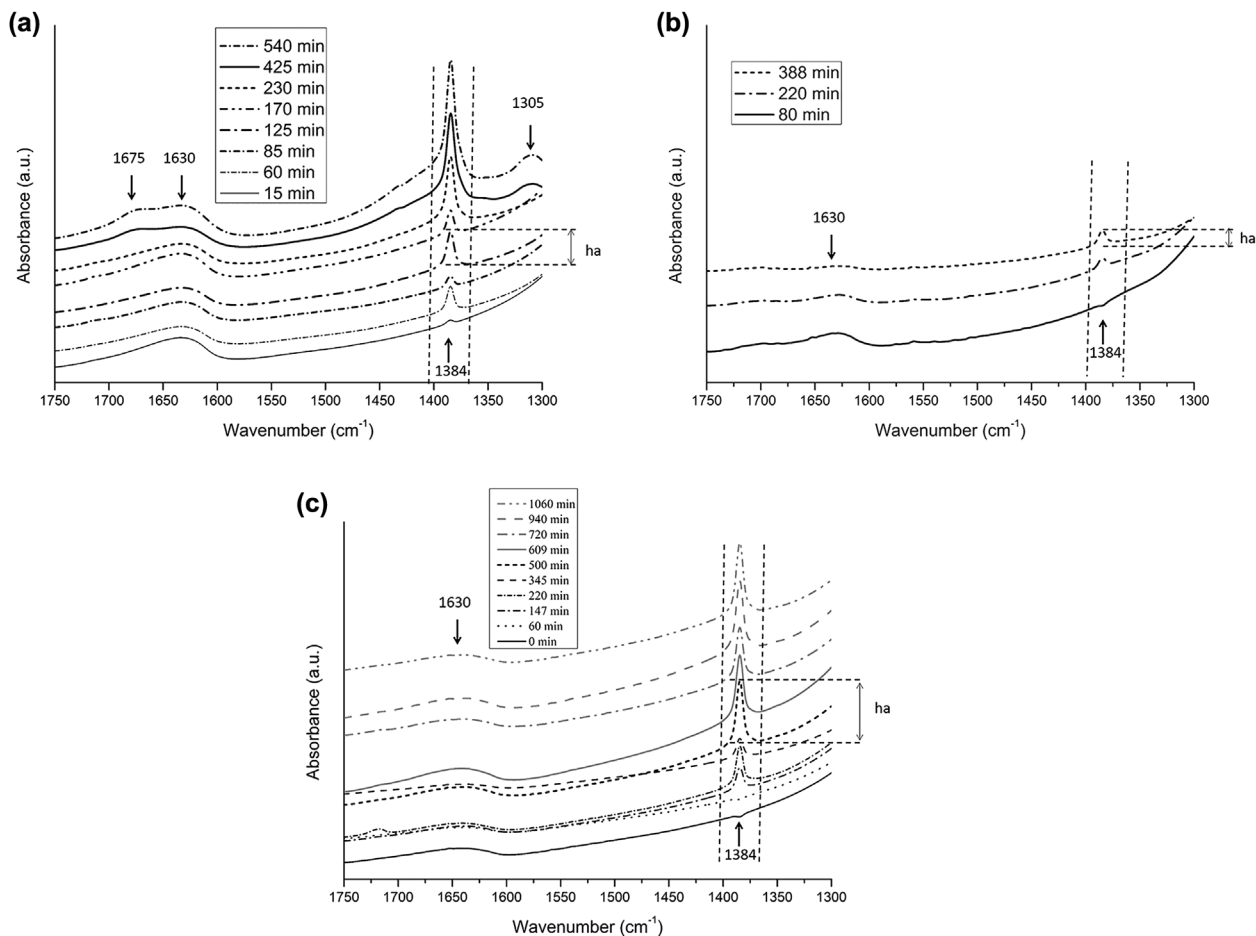


Figure 3. Evolution of FTIR spectra during ozone interaction with zeolite samples. (a) H MOR, (b) H FAU, and (c) Na MFI. Operating conditions: 38.5 g of pellet zeolites with particle size of 1.8 mm; O_{3in} : 24.7 g.m^{-3} ; HR: 0 %; F: $0.18 \text{ m}^3.\text{h}^{-1}$ at $20 \text{ }^\circ\text{C}$.

possible to experimentally distinguish the two phases in this zeolite sample.

Results obtained here indicate that during the first phase, the intensity of the band at 1384 cm^{-1} oscillates, probably because of the successive formation and disappearance of atomic oxygen surface species. This result is in agreement with previous studies

and suggests the ozone interaction with Lewis acid sites of ZSM-5 zeolites or natural zeolite, which has been described elsewhere.^[7,20] Molecular ozone is decomposed at Lewis acid sites, leading to the formation of atomic oxygen and peroxide surface species. Finally, Lewis acid sites could be regenerated and be available for a new catalytic cycle.

After the first phase, the intensity of the IR band at 1384 cm^{-1} follows a regular slight increase. Atomic species (atomic oxygen and peroxides species) are no longer formed, indicating active sites deactivation. At the end of this phase, the outlet concentration of ozone reaches the inlet value (results are not shown here) meaning that ozone decomposition at zeolite active sites has finished. It has been previously indicated that ozone decomposition over metal oxides is energetically more difficult to carry out than the adsorption step.^[38,39]

Deactivation of the H-FAU zeolite takes place faster than the Na-MFI sample (388 min versus 1060 min) even though both experiments were performed using the same inlet concentration of ozone (5.5 g.m^{-3}). Moreover, the maximum intensity of the band at 1384 cm^{-1} seems to be lower than that obtained in the case of Na-MFI (maximum height, ha, 0.04 a.u. versus 0.28 a.u.). This result suggests that a stronger interaction of ozone takes place with surface sites of Na-MFI zeolite than with surface sites of H-FAU zeolite.

Other bands are detected in the FTIR spectra. A very slight IR absorption band is always observed at 1630 cm^{-1} . This band is

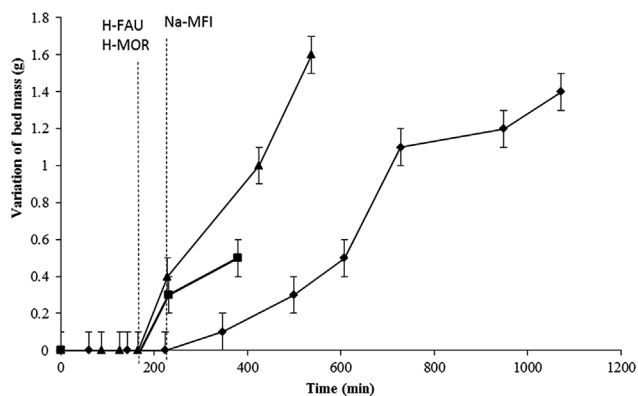


Figure 4. Variation of zeolite bed mass as a function of ozonation time: (\blacktriangle) H MOR, (\blacksquare) H FAU, (\blacklozenge) Na MFI. Operating conditions: pellet zeolites with particle size of 1.8 mm; initial mass: 38.6 g (H MOR), 46 g (H FAU), 47.7 g (Na MFI); O_{3in} : 24.8 g.m^{-3} (H MOR); 5.5 g.m^{-3} (H FAU), 5.5 g.m^{-3} (Na MFI); F: $0.18 \text{ m}^3.\text{h}^{-1}$ at $20 \text{ }^\circ\text{C}$.

related to water adsorption.^[40] As ozone removal experiments have been performed using dry air, water adsorbed on zeolite probably comes from the wafer preparation procedure. Moreover, with H-MOR, where the highest amount of ozone is decomposed (see Figure 2), two other bands have been recorded at 1305 and 1675 cm^{-1} during the second phase. They could be related to nitric acid and nitrogen dioxide adsorption at the surface of H-MOR, respectively.^[41] Since ozone is generated from air, nitrogen dioxide could be also formed. The production of nitric acid could be due to ozone reaction with nitrogen dioxide in the presence of water at surface sites of H-MOR zeolite, as has been reported in a previous study.^[41] The appearance of these contaminants could be responsible for zeolite deactivation as it is reported in the case of ozone interaction with metal oxides.^[42] These results suggest that progressive deactivation of Lewis acid sites could be mainly attributed to the formation of nitrogen contaminants (NO_x). Such nitrogen oxides come from the interaction of ozone and air taking place in the ozone generator, which could be the final responsible of poisoning active sites of zeolite surface.

The variation of zeolite bed mass as a function of ozonation time is shown in Figure 4. Two phases can also be observed for all zeolite samples. The first phase, from 0 to 220 min for H-MOR, and from 0 to 170 min for Na-MFI and H-FAU, shows an increase in the mass of zeolite bed. During this period, zeolite beds do not retain any compounds inside their pores. These results confirm that ozone is decomposed at active sites of zeolite surface. The starting point of the second phase is similar to that obtained by FTIR analysis for H-MOR and Na-MFI zeolites (170 min and 220 min, respectively). During the second phase, the mass of zeolite beds increases weakly and regularly. This trend was carefully verified, carrying out the same experiment five times. Such results are experimental evidence of the adsorption of other molecules that do not decompose and remain adsorbed. Compounds based on nitrogen such as nitric acid or nitrogen oxides could be among them.^[7] In the case of H-MOR zeolite, it seems that the progressive deactivation of Lewis acid sites is promoted by nitric acid formation at active sites zeolite surface in the presence of molecular ozone (see Figure 3). Moreover, an increase in the temperature of the reactor external wall is registered during the first phase, using an IR thermometer. This can be admitted as another proof of the catalytic activity of zeolite samples to promote ozone decomposition during this phase. However, during the second phase the outside temperature of the reactor decreases until room conditions, indicating catalyst deactivation.

Incidence of Zeolite Framework on Ozone Decomposition

Figure 5 illustrates the relationship between the amount of ozone eliminated and the concentration of Lewis acid sites (A) and available micropore volume (B).

On one hand, regardless of there being a certain trend to increase ozone elimination with the increase in the content of Lewis acid sites, it is not possible to establish a clear linear proportionality between them. On the other hand, despite a larger value of D_i in comparison with the size of ozone molecule for H-FAU and H-MOR zeolites, the amount of ozone decomposed is three times higher with the H-MOR sample than over the H-FAU sample, whereas the concentration of Lewis acid sites is quite close (67 and 91 $\mu\text{mol.g}^{-1}$ for H-FAU and H-MOR, respectively). Concerning both ZSM-5 zeolites (Na-MFI and H-MFI), their characteristics show two main variances: (i) different compensating cations (Na^+ for Na-MFI and H^+ for H-MFI); (ii) different

concentrations of Lewis acid sites (see Table 1). As discussed above (see section Characterization of As-Received Zeolites), ozone decomposition over ZSM-5 zeolite seems to be proportional to the content of Lewis acid sites. Thus, ozone decomposition would not be directly correlated to the nature of compensating cations. These results suggest that the chemical surface properties of zeolites are not the only factor affecting ozone removal. Micropore volume and its distribution provided by channels and cages should also be considered as important parameters.

As can be seen in Figure 5B, there is no linear relationship between the available micropore volume and the amount of ozone eliminated. A similar amount of ozone is decomposed over H-FAU and Na-MFI, whereas micropore volume is two times lower for Na-MFI than for H-FAU. Among zeolite characteristics, the roles of pore size and framework distribution appear to be key parameters on ozone removal. Indeed, the effects of confinement and pore selectivity seem to be determinant, as has been previously reported by Zhang et al.^[24] These authors obtain better efficiencies in the catalytic oxidation of NO_x over zeolites when the range of pore widths are in the same magnitude as NO_x molecular size.^[24] Table 1 shows the maximum diameter (D_{max}) of each zeolite. D_{max} values varies from 0.64 to 1.13 nm, being bigger than ozone molecules (0.58 nm). The highest amount of eliminated ozone is observed for a D_{max} value of 0.67 nm. Large values of D_{max} do not seem to be suitable for an efficient ozone removal, suggesting the importance of a sufficient contact distance between zeolite active surface sites and ozone molecules.

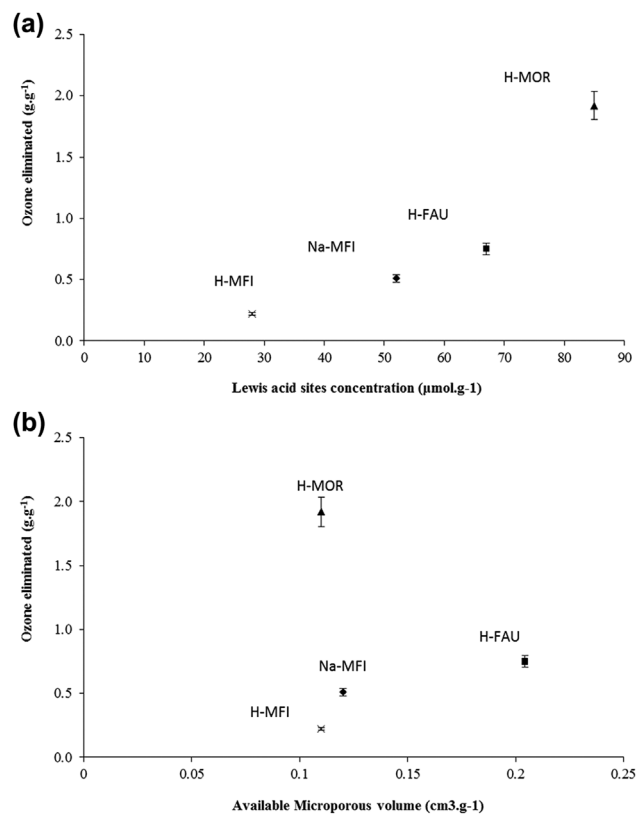


Figure 5. Influence of zeolite characteristics on ozone decomposition: (a) Effect of Lewis acid site concentration. (b) Effect of micropore volume. (▲) H MOR, (■) H FAU, (◆) Na MFI, (×) H MFI. Operating conditions: 0.1 g of ground zeolite with particle size in the range of 0.3–0.425 mm; $\text{O}_{3\text{in}}$: 15 g.m^{-3} ; F: 0.003 $\text{m}^3.\text{h}^{-1}$; 101 kPa at 20 °C.

In the case of the H-MOR zeolite, accessible micropores are located in channels with pore widths slightly larger than ozone molecules. Ozone molecules can penetrate easily into H-MOR pores. Ozone interaction with Lewis acid sites, located at the surface of zeolites, could be strengthened when the dimension of zeolite pore width matches closely to ozone molecule size.^[43] Hence, the confinement effect of the H-MOR structure probably promotes ozone decomposition reactions and Lewis sites regeneration.^[37] Unlike H-MOR, micropores of H-FAU zeolite are mainly composed of cages with a large value of D_{\max} compared to ozone molecules (1.14 versus 0.58 nm). The cages of H-FAU are probably too large to have sufficient interactions between ozone molecules and active surface sites located on the pore wall. Thus, ozone decomposition and Lewis acid site regeneration are less induced.

In the case of ZSM-5 (Na-MFI and H-MFI), the value of D_{\max} is in the same order of magnitude as ozone molecule size, allowing strong contact between ozone molecule and active surface sites located on pore walls. The effect of confinement could induce reactions of regeneration of Lewis acid sites. In spite of the fact that H-MOR and ZSM-5 (Na-MFI and H-MFI) have similar D_{\max} values and available micropore volumes (see Table 1), the observed discrepancy between both structures could be attributed to their topological differences. Channels in ZSM-5 represent 59 % of its micropore volume^[34] and their pore width is slightly lower than the size of ozone molecules. Ozone molecules could only enter ZSM-5 pores due to their structure vibrations.^[36] Thus, ozone diffusion inside this zeolite framework could be partly hindered, limiting the access of ozone molecules to inner Lewis acid sites of the zeolite surface.

Figure 6 shows the evolution of the amount of ozone eliminated as a function of the inlet concentration of ozone for all zeolites. Ozone adsorption and decomposition at Lewis acid sites could be described using the Langmuir approach, as follows:

$$q_{O_3} = \frac{K_1 Q O_3}{1 + K_1 O_3} \quad (2)$$

where q_{O_3} , K_1 , Q , and O_3 represent the total amount of ozone removed ($g_{O_3} \cdot g_{zeolite}^{-1}$), the Langmuir constant ($m^3 \cdot g_{O_3}^{-1}$), the maximum amount of ozone removed ($g_{O_3} \cdot g_{zeolite}^{-1}$), and the concentration of ozone ($g_{O_3} \cdot m^{-3}$), respectively. This proposed model is limited to zeolite samples with a particle size in the range

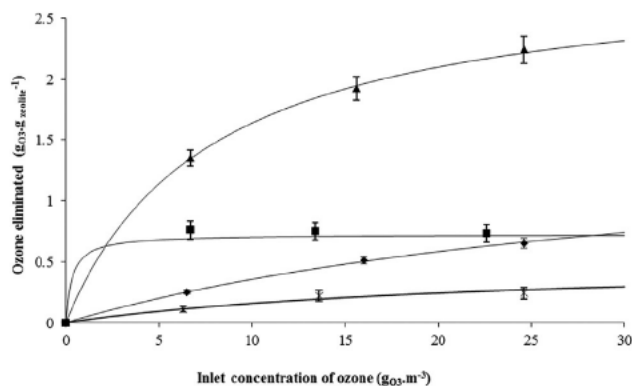


Figure 6. Influence of the inlet concentration of ozone on ozone decomposition: (▲) H MOR, (■) H FAU, (◆) Na MFI, (×) H MFI; thin line show the fitting adjust to Langmuir model for each zeolite sample. Operating conditions: 0.1 g of ground zeolite with particle size in the range of 0.3–0.425 mm; F: $0.003 \text{ m}^3 \cdot \text{h}^{-1}$; 101 kPa at $20 \text{ }^\circ\text{C}$.

of 0.3 and 0.425 mm. Other results of extrapolations to different size particles should include mass transfer diffusion resistance inside the zeolite porous structure.

As it can be seen in Figure 6, the Langmuir model fits the experimental data very well. Depending on the inlet concentration of ozone, there is a variation on the amount of ozone eliminated, as expected.^[16,38] At low inlet concentration of ozone, ozone adsorption and elimination at Lewis acid sites is very low. Under this case, Equation (2) is simplified to $q_{O_3} = K_1 Q O_3$. Whereas at high inlet concentration of ozone, ozone elimination increases, reaching a maximum value. Results shown here agree with those presented in Figure 5A. The amount of ozone eliminated is directly related to the concentration of Lewis acid sites. Zeolites with a higher amount of Lewis acid sites lead to higher ozone elimination. In the case of H-FAU zeolite, a clear plateau of ozone elimination is obtained under the experimental conditions used here. Large cavities of H-FAU zeolite facilitate ozone diffusion inside this zeolite framework, allowing reaching the maximum value of ozone elimination. However, under the same inlet concentration of ozone, the maximum values of ozone elimination are not achieved for the other zeolite samples. Such experimental results could be connected to pore width and micropore framework size distribution of each zeolite samples. Narrow channels or cages of the zeolite framework restrict ozone diffusion inside zeolite pores, limiting those zeolite samples to attain the maximum values of ozone elimination (Q) listed in Table 2. Higher concentrations of ozone are needed in order to reach the maximum value of ozone elimination.

CONCLUSIONS

Gaseous ozone decomposition was studied over four hydrophobic microporous zeolites: a Mordenite type, a Faujasite type, and two ZSM-5 types (Na-MFI and H-MFI). All zeolites tested are able to remove ozone at ambient temperature, showing different removal capacities: from 0.22 to $1.95 \text{ g}_{O_3} \cdot \text{g}_{zeolite}^{-1}$. Results reveal that both physical and chemical surface properties are important parameters in ozone elimination. The highest amount of ozone removed is attained with H-MOR, mainly for two reasons: (i) a higher Lewis acid site concentration and (ii) a more favourable structure dimension. A direct proportionality is obtained between Lewis acid site content and ozone removal, with zeolites having the same framework, namely Na-MFI and H-MFI. However, that relationship does not apply to other zeolites studied here. Thus, pore diameter and the framework distribution (channels and cages) also appear to be key factors in ozone elimination. Narrow pores having a width close to ozone molecule size promotes ozone interactions with Lewis acid sites. The confinement effect induced by narrow pores seems to be responsible for such results. Physical and chemical surface characteristics of zeolitic materials should be taken into consideration in the selection of an adequate zeolite for ozone removal from contaminated streams.

Table 2. Langmuir parameter for ozone adsorption and decomposition at Lewis acid sites of different zeolite samples

Langmuir parameters	H MOR	H FAU	Na MFI	H MFI
$K_1 \text{ (m}^3 \cdot \text{g}_{O_3}^{-1}\text{)}$	0.13	2.99	0.03	0.04
$Q \text{ (g}_{O_3} \cdot \text{g}_{zeolite}^{-1}\text{)}$	2.92	0.72	1.61	0.52
R^2	0.99	0.82	0.99	0.96

ACKNOWLEDGEMENTS

The authors gratefully acknowledge ANR (Grant No. ANR-10-ECOT-011-01), CONICYT, FONDECYT/Regular (Grant No. 1130560) and the ECOS/CONICYT Program (Grant No. C11E08), for their financial support. N. Brodu wishes to thank Mr. V. Solar from *Laboratorio de Tecnologías Limpias, Universidad Católica de la Santísima Concepción* for his valuable collaboration. H. Valdés gratefully acknowledges funding under CNRS Délégation Midi-Pyrénées contract 618035.

REFERENCES

- [1] M. S. O'Neill, D. Loomis, V. H. Borja-Aburto, *Environ. Res.* **2004**, *94*, 234.
- [2] C. Jiang, P. Zhang, B. Zhang, J. Li, M. Wang, *Ozone-Sci. Eng.* **2013**, *35*, 308.
- [3] G. Actis Grande, G. Rovero, S. Sicardi, M. Giansetti, *Can. J. Chem. Eng.* **2017**, *95*, 297.
- [4] J. N. Cape, *Sci. Total Environ.* **2008**, *400*, 257.
- [5] H. Valdés, M. Sánchez-Polo, J. Rivera-Utrilla, C. A. Zaror, *Langmuir* **2002**, *18*, 2111.
- [6] H. Einaga, S. Futamura, *Catal. Commun.* **2007**, *8*, 557.
- [7] S. Alejandro, H. Valdés, C. A. Zaror, *J. Adv. Oxid. Technol.* **2011**, *14*, 182.
- [8] C. Subrahmanyam, D. A. Bulushev, L. Kiwi-Minsker, *Appl. Catal. B-Environ.* **2005**, *61*, 98.
- [9] T. Merle, J. S. Pic, M. H. Manero, H. Debellefontaine, *Water Sci. Technol.* **2009**, *60*(11), 2921.
- [10] T. Batakliiev, G. Tyuliev, V. Georgiev, M. Anachkov, A. Eliyas, S. Rakovsky, *Ozone-Sci. Eng.* **2015**, *37*, 216.
- [11] N. Kumar, P. Konova, A. Naydenov, T. Heikillä, T. Salmi, D. Murzin, *Catal. Lett.* **2004**, *98*, 57.
- [12] N. Kumar, P. Konova, A. Naydenov, T. Salmi, D. Y. Murzin, T. Heikilla, V. P. Lehto, *Catal. Today* **2007**, *119*, 342.
- [13] H. Einaga, A. Ogata, *J. Hazard. Mater.* **2009**, *164*, 1236.
- [14] P. Nikolov, K. Genov, P. Konova, K. Milenova, T. Batakliiev, V. Georgiev, S. Rakovsky, *J. Hazard. Mater.* **2010**, *184*, 16.
- [15] P. Konova, A. Naydenov, P. Nikolov, F. Klingstedt, N. Kumar, *J. Mater. Sci.* **2011**, *46*, 7129.
- [16] M. Sugawara, A. Ogata, *Ozone-Sci. Eng.* **2011**, *33*, 158.
- [17] E. Rezaei, J. Soltan, *Chem. Eng. J.* **2012**, *198-199*, 482.
- [18] P. Monneyron, M.-H. Manero, S. Manero, *Can. J. Chem. Eng.* **2007**, *85*, 326.
- [19] C. W. Kwong, C. Y. H. Chao, K. S. Hui, M. P. Wan, *Environ. Sci. Technol.* **2008**, *42*, 8504.
- [20] N. Brodu, M.-H. Manero, C. Andriantsiferana, J. S. Pic, H. Valdés, *Chem. Eng. J.* **2013**, *231*, 281.
- [21] H. Valdés, S. Alejandro, C. A. Zaror, *J. Hazard. Mater.* **2012**, *227-228*, 34.
- [22] K. Thomas, P. E. Hoggan, L. Mariey, J. Lamotte, J. C. Lavalley, *Catal. Lett.* **1997**, *46*, 77.
- [23] B. Dhandapani, S. T. Oyama, *Appl. Catal. B-Environ.* **1997**, *11*, 126.
- [24] Z. Zhang, J. D. Atkinson, B. Jiang, M. J. Rood, Z. Yan, *Appl. Catal. B-Environ.* **2015**, *163*, 573.
- [25] D. W. Breck, *Zeolite Molecular Sieves: Structure, Chemistry and Use*, John Wiley & Sons, New York 1974.
- [26] F. Rouquérol, J. Rouquerol, K. Sing, *Adsorption by powders and porous solids: principles, methodology and applications*, Academic Press, Cambridge 1998.
- [27] C. Baerlocher, L. McCuske, "Database of Zeolite Structures," *Structure Commission of the International Zeolite Association 2017*, accessed on 6 June 2017, <http://www.iza-structure.org/databases/>.
- [28] M. Guisnet, F. Ribeiro, *Les zéolithes: un nanomonde au service de la catalyse*, EDP Sciences, Les Ulis 2006.
- [29] E. First, C. Gounaris, J. Wei, C. A. Floudas, *Phys. Chem. Chem. Phys.* **2011**, *13*, 17339.
- [30] E. P. Barrett, L. G. Joyner, P. P. Halenda, *J. Am. Chem. Soc.* **1951**, *73*, 373.
- [31] G. Horvath, K. Kawazoe, *J. Chem. Eng. Jpn.* **1983**, *16*, 470.
- [32] M. Guisnet, P. Ayrault, C. Coutanceau, M. Fernanda Alvarez, J. Datka, *J. Chem. Soc. Faraday T.* **1997**, *93*, 1661.
- [33] S. Alejandro, H. Valdés, M.-H. Manéro, C. A. Zaror, *J. Hazard. Mater.* **2014**, *274*, 212.
- [34] C. Y. H. Chao, C. W. Kwong, K. S. Hui, *J. Hazard. Mater.* **2007**, *143*, 118.
- [35] M. M. J. Treacy, M. D. Foster, *Micropor. Mesopor. Mater.* **2009**, *118*, 106.
- [36] R. Roque Malherbe, R. Wendelbo, *Thermochim. Acta* **2003**, *400*, 165.
- [37] T. K. Phung, L. P. Hernández, A. Lagazzo, G. Busca, *Appl. Catal. A-Gen.* **2015**, *493*, 77.
- [38] W. Li, S. T. Oyama, *J. Am. Chem. Soc.* **1998**, *120*, 9047.
- [39] R. C. Sullivan, T. Thornberry, J. P. D. Abbatt, *Atmos. Chem. Phys.* **2004**, *4*, 1301.
- [40] J. B. Lowenstern, B. W. Pitcher, *Am. Mineral.* **2013**, *98*, 1660.
- [41] A. Gal, A. Ogata, S. Futamura, K. Mizuno, *J. Phys. Chem. A* **2004**, *108*, 7003.
- [42] A. E. Michel, C. R. Usher, V. H. Grassian, *Atmos. Environ.* **2003**, *37*, 3201.
- [43] H.-B. Zhang, K. Zhang, Z.-Y. Yuan, W. Zhao, H.-X. Li, *J. Nat. Gas Chem.* **1997**, *6*, 228.